Mapana – Journal of Sciences
2022, Vol. 21, No. 3, 00-00
ISSN 0975-3303/https://doi.org/10.12723/mjs.62.0

Corrosion characteristics of $BaTiO_3$ perovskite coatings on AZ31 alloy

Y L Raja Mohan* & A Cyril†

Abstract

In this work, we have synthesized $BaTiO_3$ perovskite material by the hydrothermal procedure. The synthesized $BaTiO_3$ perovskite material was characterized by XRD and FTIR analysis. The XRD study reveals high crystalline nature, and the FTIR analysis shows the presence of –OH and CH functional groups. The $BaTiO_3$ perovskite material was mixed with silicone resin and coated over AZ31 by the doctor blade method and dried in an oven at 90 ^oC. The coating was cured for 2-6 h before commencing the electrochemical analysis. The coated samples were mounted with copper electrical wire and used as an anode or working electrode in 3.5% NaCl electrolyte, wherein platinum foil as the counter electrode and saturated calomel electrode (SCE) as the reference electrode. Initially, open circuit potential was recorded and preceded by electrochemical impedance (EIS) measurements. Finally, a linear sweep voltammogram or Tafel plot was recorded, and data were plotted. It is noticed that the OCP was -0.25 V (vs SCE), and corrosion current density was found around 6 $x10^{-7}$ A/cm^2. The results reveal that perovskite-based $BaTiO_3$ coatings demonstrated a noble shift in the corrosion potential of AZ31 alloys in the NaCl medium. The presence of silicone

* Department of Industrial Chemistry, Alagappa University, Karaikudi, Tamil Nadu, India; Email ID
† Post graduate & Research Department of Chemistry, Raja Dorasingam Government Arts College, Sivaganga, Tamilnadu, India; cyrilchemistry@gmail.com

resin played a vital role in developing homogeneous $BaTiO_3$ perovskite material coatings over AZ31 alloy.

Keywords: Mg alloys; AZ31; $BaTiO_3$, Silicone resin, Corrosion

1. Introduction

Magnesium alloys are being used well in many applications due to the specific properties such as light weight, high strength with low density (1.7 g/cm^3). The Mg alloys are widely used in the manufacturing of aerospace, automotive components and industrial equipment, which include steering wheels, seat frames and transmission cases in automobile industries, airframes and internal components in aerospace sectors, etc. [1, 2]. Due to the more negative electromotive force, the Mg and its alloys suffer with higher corrosion rates [3, 4]. Many attempts have been made to improve the Mg and its alloys corrosion resistance in an aqueous medium [5-12]. Among all the surface modifications by the application of coatings found a commercially feasible method to improve the corrosion resistance and protect the Mg alloys [13-15]. The tungsten carbide coatings were developed by plasma electrolytic oxidation process on Mg alloy (AZ31), wherein the WC coatings showed noble shift [13]. Further, Wu et al. developed diamond like carbon (DLC) coatings on AZ31 alloy, which showed excellent corrosion resistance [14]. Similarly, Han et al. developed Graphene based coatings and demonstrated shift in the positive direction of -1.15 V (SCE) in 3.5% NaCl electrolyte [15].

More recently, Zhang et al. [16] developed PEO/Mg-Al layered double hydroxide (LDH) coatings on AZ31 alloy using one-step plasma electrolytic oxidation (PEO) method. Aluminum and Zinc enriched nanometer thick layer formed at the substrate and PEO coating, which in turn showed an enhancement in the corrosion resistance for AZ31 alloy. Similarly, Zahedi et al. formulated a composite coating of the Zn–Ce LDH/oxide on AZ31 and demonstrated enhanced corrosion protection [17]. Mashtalyar et al. developed a process to incorporate ZrO_2/SiO_2 nanomaterial in the PEO layers and identified that the incorporation of nanomaterials showed enhanced corrosion protection in Mg alloys [18].

Most of the works related to the research work on the corrosion-resistant coating for Mg alloy have not studied the corrosion behavior on perovskite oxides $BaTiO_3$ of AZ31 alloy. In this work, $BaTiO_3$ perovskite material synthesized by simple hydrothermal route. The $BaTiO_3$electrode was prepared by the following procedure. Initially, the $BaTiO_3$material was mixed with silicone resin and coated over AZ31 using doctor blade method and dried. The coated samples were used as working electrode in 3.5% NaCl electrolyte, wherein platinum and saturated calomel electrode (SCE) foil were used as counter electrode and reference electrodes, respectively. The results reveal that perovskite based $BaTiO_3$ coatings demonstrated a noble shift in the corrosion potential of AZ31 alloys in NaCl medium. The presence of silicone resin played a vital role in developing homogeneous $BaTiO_3$ perovskite material coatings over AZ31 alloy.

2. Materials & Methods

2.1. Chemicals

The chemicals such as barium hydroxide (Ba $(OH)_2$ H_2O, CAS NO: 22326-55-2), titanium chloride ($Ti(OH)_4$, CAS NO: 7550-45-0)were purchased from Merck and Silicone resin 1805was purchased from Dow Corning.

2.2. BaTiO3 synthesis

$BaTiO_3$ nanoparticles were synthesized via hydrothermal route. 10 mmol of each barium hydroxide and titanium chloride are dissolved separately in distilled water and mixed together under stirring. Further, 10 mol NaOH solution was added to adjust the pH=13 of the above solution and transferred into a 50 ml capacity Teflon-lined stainless-steel autoclave and dried.

2.3. AZ31 Sample preparation

The AZ31 samples were cut into 11 x 11 x 3 mm size using wire EDM process. The samples were polished using SiC grit paper, wherein the polishing procedure stars with the initial 200 SiC grit paper and went up to 1200 grit and finally 1- and 0.5-micron diamond paste polishing with cloth. The samples were washed

with non-polar solvent (Diethyl ether) to remove the polishing impurities.

2.4. Electrode preparation

The perovskite oxide powder of $BaTiO_3$(1 g) was added to silicone resin (10 ml)and mixed well. The paste was then applied on the AZ31 alloy by doctor blade method. The coated samples were dried in oven before commencing the electrochemical studies.

2.5. Electrochemical experiments

The corrosion resistance of bare AZ31 alloy and $BaTiO_3$ perovskite oxide coated AZ31 alloy was analyzed using three electrode based electrochemical system, wherein the coated AZ31 alloy as working electrode, platinum foil as counter electrode and saturated calomel electrode (SCE), while 3.5% NaCl electrolyte.

2.6. Instrumentation of characterization studies

X-ray diffraction pattern was recorded on an (XRD Bruker D8-Advanced, Germany) angle between 10 °- 90 ° angle with 6 ° per min. FT-IR (Fourier Transform Infrared spectroscopy) were obtained through transmittance data on an FT-IR spectrometer (Bruker Tensor 27). Samples were analyzed by using HRTEM (High-Resolution Transmission Electron Microscope) (Tecnai F20 S-TWIN TMP, Netherlands) with a resolution 0.144nm. Electrochemical workstation PARSTAT 2273 with power suite. ZEISS field emission scanning electron microscope (FESEM) is used for surface analysis.

3. Results & Discussion

3.1. X-ray diffraction analysis

The crystallinity and phase purity of bare AZ31 and $BaTiO_3$ perovskite oxide coated AZ31 alloy were analyzed by X-ray diffraction analysis and presented in Figures 1 and 2.

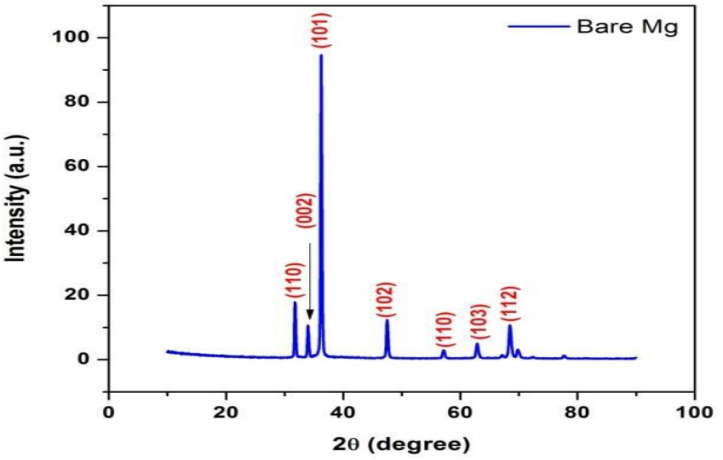

Figure 1: X- ray diffraction pattern of AZ31 alloy

The obtained X-ray diffraction peaks for bare AZ31 alloy are well matched with the standards (JCPDS file no 35-0821) hexagonal crystal structure that belongs to P63/mmc space group for Mg alloy (a=b=3.2094 Å and c=5.211Å) [19-21].

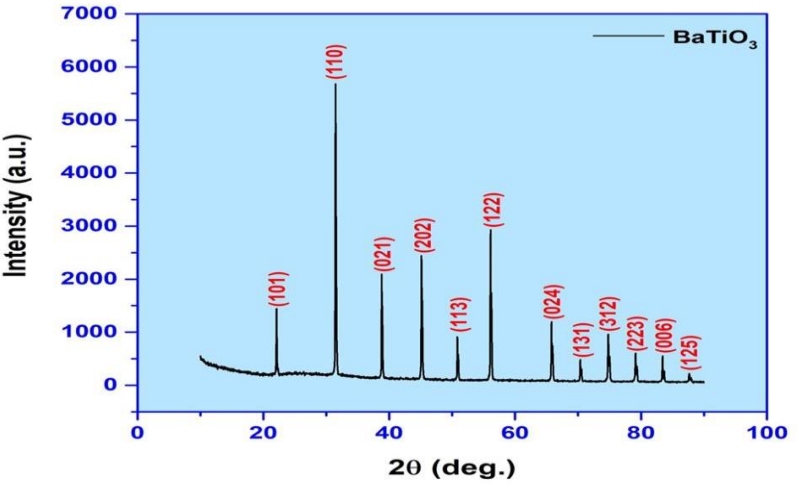

Figure 2: X- ray diffraction pattern of $BaTiO_3$ perovskite oxide coated AZ31 alloy

Figure 2 demonstrate the high crystallinity of $BaTiO_3$ perovskite oxide coating with most preferential (110) plane. The other peaks (1 0 1), (0 2 1), (2 0 2), (1 1 3), (1 2 2), (0 2 4), (1 3 1), (3 1 2), (2 2 3), (0 0 6) and (1 2 5) exhibiting a perovskite crystal structure with tetragonal symmetry (a = b = 3.9940 Å and c = 4.0380 Å)and belongs to P4mm space group [23 - 24].

4. Surface morphology

4.1. Surface morphology

The surface morphology of $BaTiO_3$ perovskite oxide is shown in Figures 3-5. It is noticed that the nano particles are well distributed. The shape of the particles is irregular and the size is varied among them.

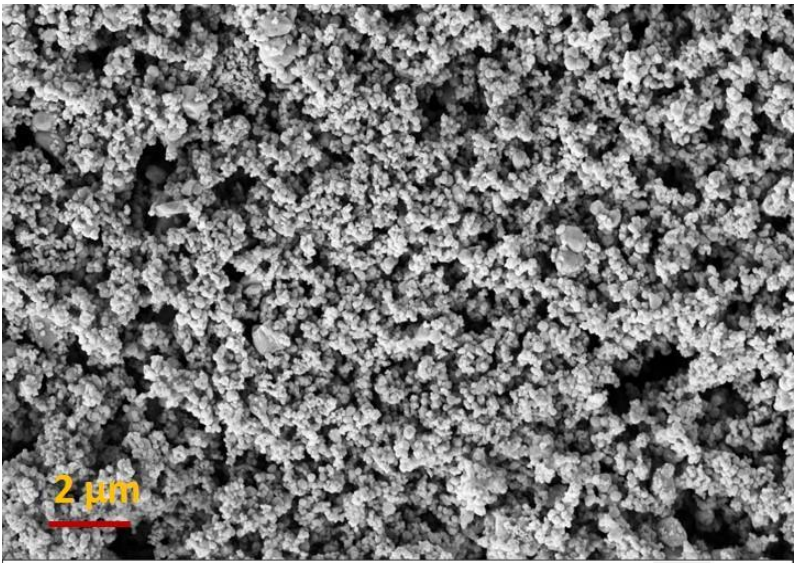

Figure 3: Surface morphology of $BaTiO_3$ perovskite oxide

The higher magnified images showing the surface morphology of $BaTiO_3$ perovskite oxide show distinct features, which includes nano sized particles. The crystal growth shows there is no much effect of surfactant in the synthesis of $BaTiO_3$ perovskite oxide. As mentioned in the XRD analysis, the powders are free from impurities and the figures show the shape and size of particles, which corresponds to purely $BaTiO_3$ perovskite oxide. In many

applications, the nano-sized particles provide better performance, however, in the current study, the nano sized particles provided high dense packing in the coatings.

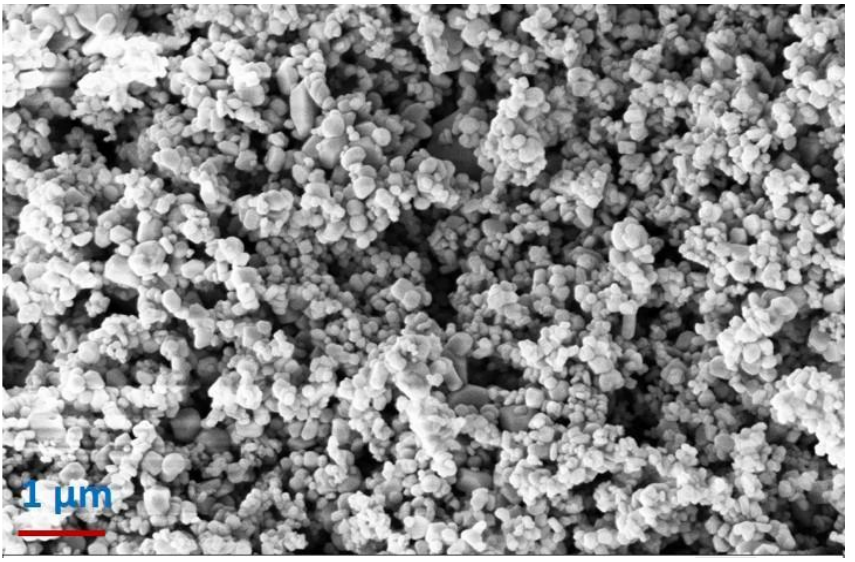

Figure 4: Surface morphology of $BaTiO_3$ perovskite oxide at higher magnification

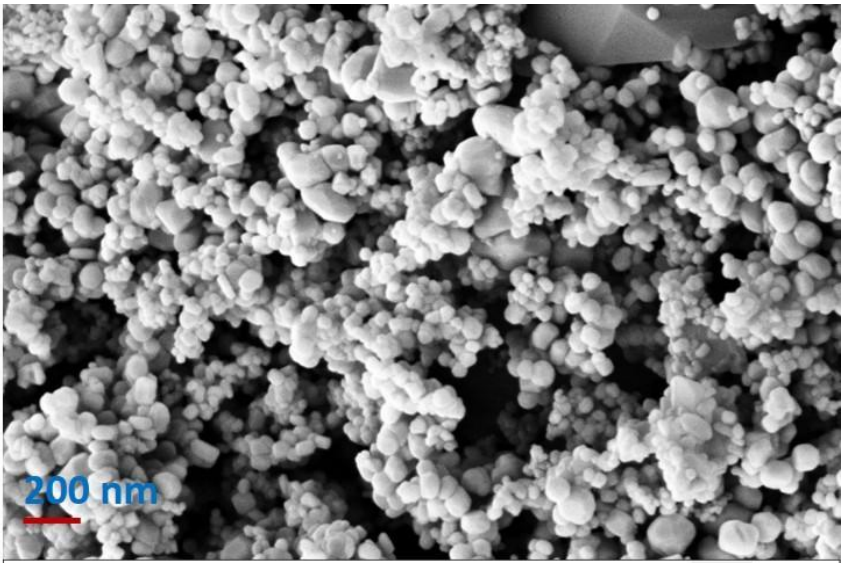

Figure 5: Surface morphology of $BaTiO_3$ perovskite oxide at higher magnification

4.2. HRTEM analysis

The morphological images acquired through high resolution transmission electron microscope images is shown in Figure 6.

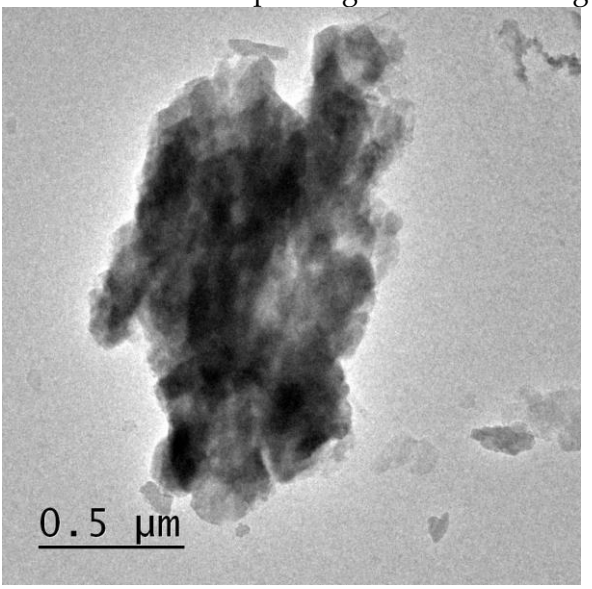

Figure 6: HRTEM images of $BaTiO_3$ perovskite oxide

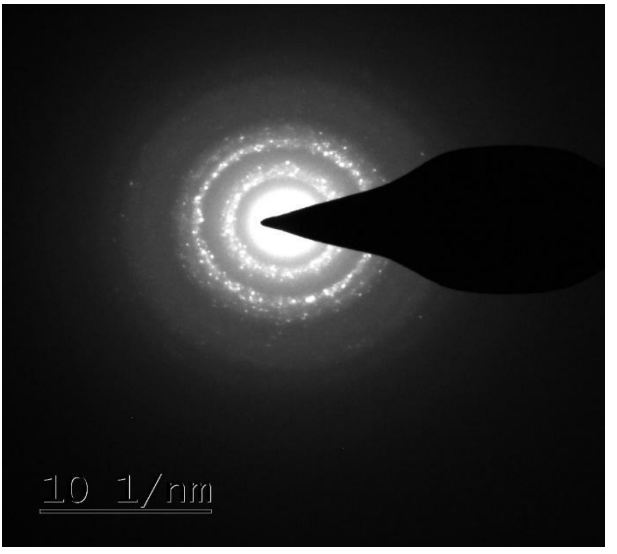

Figure 7: SAED of BaTiO3 perovskite oxide

The Figure 6 reveals that the nanoparticles are clubbed together and showed as micro-sized particle. However, the individual particles are clearly demonstrating the nanosized nature in high-resolution transmission electron microscopic analysis. The $BaTiO_3$ perovskite oxidepowder was sonicated and deposited on the Cu grid and examined the morphological features in HRTEM. The Figure 7 reveals the polycrystallinity nature.

4.3. FTIR analysis

The Fourier Transform Infrared Spectroscopy (FTIR) analysis of $BaTiO_3$ perovskite oxideis shown in Figure 8.

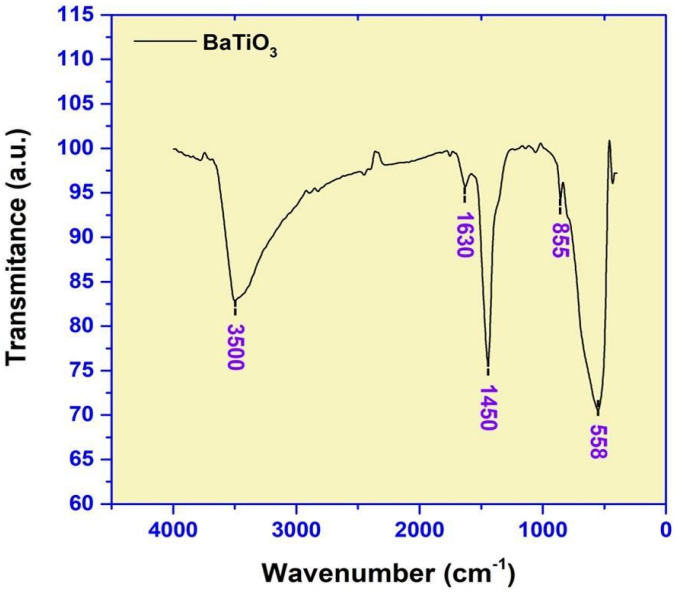

Figure 8: FTIR spectrum of $BaTiO_3$ perovskite oxide

It is noticed that the peaks at 558, 1450, 1630 and 3500 cm-1. The band at 558 cm-1 is attributed to the stretching mode of Ti-O. The bands at 1450 is correspond to the vibration C-O in -CO32- due to presence trace BaCO3 [25, 26]. This attributed to the CO2 solubility in high alkaline medium that eventually reacted with Barium to form barium carbonate. This is high un-avoidable reaction due to

the carbon dioxide entrapment during the chemical reaction in hydrothermal system. The band at 3500 cm-1 corresponds to O-H group and a peak at 1626 cm-1 corresponds to the bending mode of H-O-H resulted from physically adsorbed water.

4.4. Electrochemical analysis

The corrosion potentials of bare AZ31 alloy and $BaTiO_3$ perovskite oxide coated AZ31 alloy are shown in Figure 9.

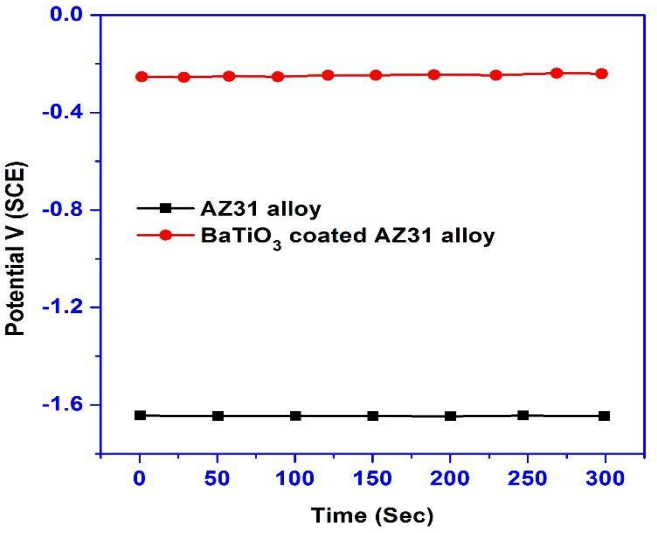

Figure 9: Open circuit potentials of bare AZ31 and $BaTiO_3$ perovskite oxide coated AZ31 alloy

From the figure, it is noticed that the bare AZ31 alloy shows a corrosion potential around -1.65 V (SCE), while $BaTiO_3$ perovskite oxide coated AZ31 alloy shows a corrosion potential of around -1.25 V (SCE). This feature clearly indicate that the perovskite coating is beneficial as the corrosion potential shifted to more noble direction, which shows the higher corrosion protection induced due to the coating.

The corrosion characteristics of bare AZ31 alloy and $BaTiO_3$ perovskite oxide coated AZ31 alloy were studied and the corrosion behavior observed from the recorded Tafel plots. The Tafel plot of bare AZ31 alloy is shown in Figure 10.

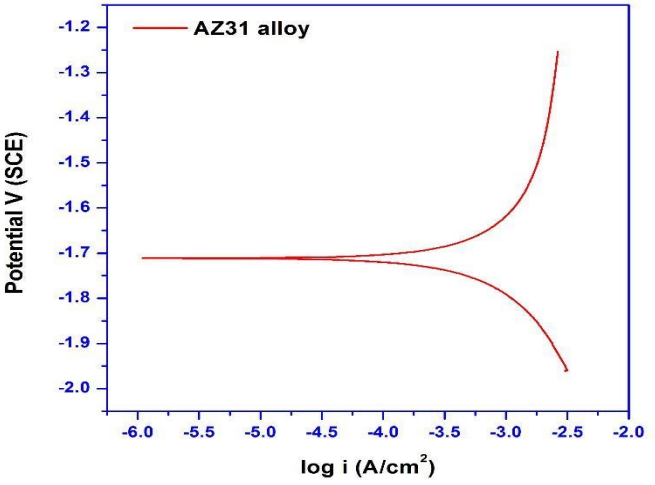

Figure 10: Tafel plot of bare AZ31 alloy.

From the Figure 10, it is noticed that corrosion potential is noticed that bare AZ31 demonstrated the corrosion rate 3.4 x 10^{-4} A/cm^2.

Similarly, the Tafel plot of $BaTiO_3$ perovskite oxide coated AZ31 alloy is shown in Figure 11. From the Figure, it is noticed that corrosion potential is noticed that $BaTiO_3$ perovskite oxide coated AZ31 demonstrated the corrosion rate 6 x10^{-7} A/cm^2.

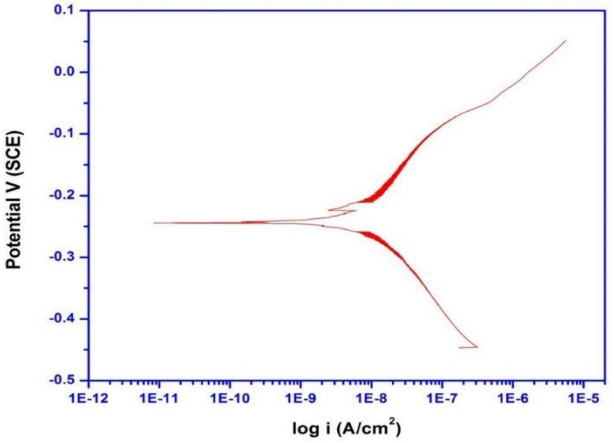

Figure 11: Tafel plot of $BaTiO_3$ perovskite oxide coated AZ31 alloy.

The electrochemical impedance spectroscopy (EIS)curves of bare AZ31 and BaTiO3 perovskite oxide coated AZ31 alloyin 3.5 % NaCl solution is shown in Figure 12.

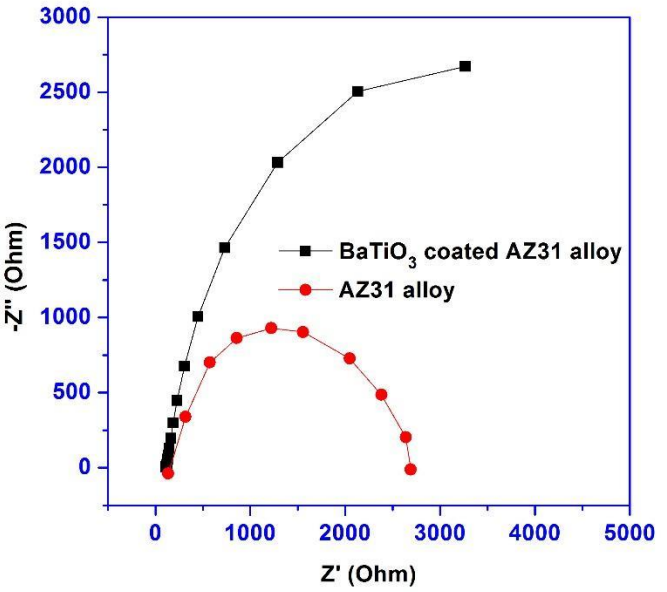

Figure 12: Electrochemical impedance curves of bare AZ31 and $BaTiO_3$ perovskite oxide coated AZ31 alloy

The EIS studies show that bare AZ31 alloy showed very less corrosion resistance, and $BaTiO_3$ perovskite oxide coated AZ31 alloy showed superior corrosion resistance.

5. Conclusion

- The $BaTiO_3$ perovskite oxide was synthesized using a simple hydrothermal process
- The $BaTiO_3$ perovskite oxide coatings were developed on AZ31 alloy using silicone resin
- The bare AZ31 alloy showed corrosion potential Ecorr of -1.65 V (SCE) and demonstrated 3.4 x 10^{-4} A/cm^2, while

$BaTiO_3$ perovskite oxide coated AZ31 alloy exhibited6 $x10^{-7}$ A/cm^2.

- The results reveal that the $BaTiO_3$ perovskite oxide coated AZ31 alloy demonstrated higher corrosion resistance than of bare AZ31 alloy

References

[1] Mordike, B. L. and Ebert, T. (2001) Magnesium: Properties-Applications-Potential, Materials Science and Engineering A, 302 (1), 37-45.

[2] Thomas, S., Medhekar, N. V., Frankel, G. S., and Birbilis, N. (2015). Corrosion mechanism and hydrogen evolution on Mg. Current Opinion in Solid State and Materials Science, 19(2), 85–94.

[3] Wu, R., Yan, Y., Wang, G., Murr, L. E., Han, W., Zhang, Z., & Zhang, M. (2014). Recent progress in magnesium–lithium alloys. International Materials Reviews, 60(2), 65–100.

[4] Tokunaga, T., Ohno, M., and Matsuura, K. (2018). Coatings on Mg alloys and their mechanical properties: A review. Journal of Materials Science & Technology, 34(7), 1119–1126.

[5] Singh Raman, R. K., Birbilis, N., & Efthimiadis, J. (2004). Corrosion of Mg alloy AZ91 – the role of microstructure. Corrosion Engineering, Science and Technology, 39(4), 346–350.

[6] Esmaily, M., Shahabi-Navid, M., Svensson, J.-E., Halvarsson, M., Nyborg, L., Cao, Y., and Johansson, L.-G. (2015). Influence of temperature on the atmospheric corrosion of the Mg–Al alloy AM50. Corrosion Science, 90, 420–433.

[7] Esmaily, M., Blücher, D. B., Lindström, R. W., Svensson, J.-E., & Johansson, L. G. (2015). The Influence of SO2on the Corrosion of Mg and Mg-Al Alloys. Journal of The Electrochemical Society, 162(6), C260–C269.

[8] Pu, Z., Yang, S., Song, G.-L., Dillon, O. W., Puleo, D. A., and Jawahir, I. S. (2011). Ultrafine-grained surface layer on Mg–Al–Zn alloy produced by cryogenic burnishing for enhanced corrosion resistance. Scripta Materialia, 65(6), 520–523.

[9] Danaie, M., Asmussen, R. M., Jakupi, P., Shoesmith, D. W., & Botton, G. A. (2013). The role of aluminum distribution on the local corrosion resistance of the microstructure in a sand-cast AM50 alloy. Corrosion Science, 77, 151–163.

[10] Asmussen, R. M., Jakupi, P., Danaie, M., Botton, G. A., & Shoesmith, D. W. (2013). Tracking the corrosion of magnesium sand cast AM50 alloy in chloride environments. Corrosion Science, 75, 114–122.

[11] Shahabi-Navid, M., Esmaily, M., Svensson, J.-E., Halvarsson, M., Nyborg, L., Cao, Y., & Johansson, L.-G. (2014). NaCl-Induced Atmospheric Corrosion of the MgAl Alloy AM50-The Influence of CO2. Journal of The Electrochemical Society, 161(6), C277–C287.

[12] Kwon, J., Baek, S.-M., Jung, H., Kim, J. C., Lee, S.-Y., & Park, S. S. (2021). Role of microalloyed Sm in enhancing the corrosion resistance of hot-rolled Mg–8Sn–1Al–1Zn alloy. Corrosion Science, 185, 109425.

[13] Li, J., Xie, D., Yu, H., Liu, R., Shen, Y., Jiang, H.,Qin, G. (2020). Microstructure and mechanical property of multi-pass low-strain rolled Mg-Al-Zn-Mn alloy sheet. Journal of Alloys and Compounds, 155228.

[14] Wu, G., Dai, W., Zheng, H., & Wang, A. (2010). Improving wear resistance and corrosion resistance of AZ31 magnesium alloy by DLC/AlN/Al coating. Surface and Coatings Technology, 205(7), 2067–2073.

[15] Han, B. (2017). A Composite Anodic Coating Containing Graphene on AZ31 Magnesium Alloy. International Journal of Electrochemical Science, 9829–9843.

[16] Xinxin Zhang, Yupeng Zhang, You Lv, Zehua Dong, Teruo Hashimoto, Xiaorong Zhou 2022. Enhanced corrosion resistance of AZ31 Mg alloy by one-step formation of PEO/Mg-Al LDH composite coating. doi.org/10.1016/j.corcom.2022.05.001

[17] Luo, A., Pekguleryuz, M., Agnew, S., Allison, J., Kainer, K., Nyberg, E., Yue, S. (Eds.). (2021). Magnesium 2021. The

Minerals, Metals & Materials Series. doi:10.1007/978-3-030-72432

[16] Mashtalyar, D. V., Imshinetskiy, I. M., Nadaraia, K. V., Gnedenkov, A. S., Sinebryukhov, S. L., Ustinov, A. Y., Gnedenkov, S. V. (2021). Influence of ZrO2/SiO2 nanomaterial incorporation on the properties of PEO layers on Mg-Mn-Ce alloy. Journal of Magnesium and Alloys. doi:10.1016/j.jma.2021.04.013

[19] Avedesian, M.M., Baker, H. (1999). ASM Specialty Handbook, Magnesium and Magnesium Alloys, ASM International, USA.

[20] Uddin, M. S., Hall, C., & Murphy, P. (2015). Surface treatments for controlling corrosion rate of biodegradable Mg and Mg-based alloy implants. Science and Technology of Advanced Materials, 16(5), 053501.

[21] Fridrich, H.E., Mordike, B.L. (2006). Magnesium Technology, Springer, Germany.

[22] Sunil, B. R., Ganesh, K. V., Pavan, P., Vadapalli, G., Swarnalatha, C., Swapna, P., Pradeep Kumar Reddy, G. (2016). Effect of aluminum content on machining characteristics of AZ31 and AZ91 magnesium alloys during drilling. Journal of Magnesium and Alloys, 4(1), 15–21.

[23] Li, L., & Nam, N. D. (2016). Effect of yttrium on corrosion behavior of extruded AZ61 Mg alloy. Journal of Magnesium and Alloys, 4(1), 44–51.

[24] Saikrishna, N., Pradeep Kumar Reddy, G., Munirathinam, B., & Ratna Sunil, B. (2016). Influence of bimodal grain size distribution on the corrosion behavior of friction stir processed biodegradable AZ31 magnesium alloy. Journal of Magnesium and Alloys, 4(1), 68–76.

[25] Ramajo, L., Catro, M.S. and Reboredo, M.M. (2007) Effect of Silane as Coupling Agent on the Dielectric Properties of BaTiO3-Epoxy Composites. Composites Part A: Applied Science and Manufacturing, 38, 1852-1959.

[26] Marciniec, B., Krysztafkiewicz, A., & Domka, L. (1983). Wettability of silane films on silica fillers. Colloid and Polymer Science, 261(4), 306–311.